Published in final edited form as:
Chem Eng J. 2011 June 1; 170(2-3): 547–554. doi:10.1016/j.cej.2011.01.099.

Nanosilver on nanostructured silica: Antibacterial activity and Ag surface area

Georgios A. Sotiriou, **Alexandra Teleki**[1], **Adrian Camenzind**[2], **Frank Krumeich**, **Andreas Meyer**[3], **Sven Panke**[3], and **Sotiris E. Pratsinis**[*]

Particle Technology Laboratory, Institute of Process Engineering, Department of Mechanical and Process Engineering, Sonneggstrasse 3, CH-8092 Zurich

[3]Bioprocess Laboratory, Department of Biosystems Science and Engineering, Mattenstrasse 26, CH-4058 Basel, ETH Zurich, Switzerland

Abstract

Nanosilver is one of the first nanomaterials to be closely monitored by regulatory agencies worldwide motivating research to better understand the relationship between Ag characteristics and antibacterial activity. Nanosilver immobilized on nanostructured silica facilitates such investigations as the SiO_2 support hinders the growth of nanosilver during its synthesis and, most importantly, its flocculation in bacterial suspensions. Here, such composite Ag/silica nanoparticles were made by flame spray pyrolysis of appropriate solutions of Ag-acetate or Ag-nitrate and hexamethyldisiloxane or tetraethylorthosilicate in ethanol, propanol, diethylene glucolmonobutyl ether, acetonitrile or ethylhexanoic acid. The effect of solution composition on nanosilver characteristics and antibacterial activity against the Gram negative *Escherichia coli* was investigated by monitoring their recombinantly synthesized green fluorescent protein. Suspensions with identical Ag mass concentration exhibited drastically different antibacterial activity pointing out that the nanosilver surface area concentration rather than its mass or molar or number concentration determine best its antibacterial activity. Nanosilver made from Ag-acetate showed a unimodal size distribution, while that made from inexpensive Ag-nitrate exhibited a bimodal one. Regardless of precursor composition or nanosilver size distribution, the antibacterial activity of nanosilver was correlated best with its surface area concentration in solution.

Keywords

E. coli toxicity; bactericidal activity; silver ions; silver nanoparticles

1. Introduction

Nanosilver is used already in heterogeneous catalysis [1] and finds new applications in textiles [2], biomedical devices [3], biodegradable polymer films for food packaging [4], biological labeling [5], plasmon photonics and color [6], optoelectronics and surface enhanced Raman scattering (SERS) [7]. At the same time, the disposal of nanosilver raises concerns for its toxicity against aquatic micro-organisms and therefore draws public

[*]Corresponding author: pratsinis@ptl.mavt.ethz.ch.
[1]Currently at DSM Nutritional Products, Basel, Switzerland
[2]Currently at Optotune AG, Dubendorf, Switzerland

Europe PMC Funders Author Manuscripts

attention [8]. In fact, nanosilver is one of the first nanomaterials to be regarded toxic and petitions had been filed to the U. S. Environmental Protection Agency (EPA) to regulate it as a pesticide [9]. Therefore to safely employ nanosilver in commercial products, correct risk and dose relations need to be determined [10-12].

The properties of nanosilver particles may change depending on their size hindering, therefore, the correct assessment of such dose relations [10]. Smaller nanosilver particles are more toxic than larger ones especially when oxidized [13,14]. Even though metallic silver is practically insoluble in water [15], when present in nanometer size range, Ag^+ ions are released (leached) from its surface [13,16,17]. The antibacterial activity of small (<10 nm) nanosilver particles is dominated by Ag^+ ions, while for larger ones (>15 nm) the antibacterial contribution by Ag^+ ions and particles is comparable [18]. Such a behavior implies a surface area dependency of the antibacterial activity especially for small nanosilver sizes since the Ag^+ ion release is proportional to the exposed nanosilver surface area [18]. This dependency could not be proven when evaluating [10] data of plasma-made nanosilver and macrophages cells [19]. Toxicological studies, however, of other engineered nanoparticles (e.g. TiO_2) show this surface dependency [20]. So and it has been suggested that dose relations expressed in surface area concentration may reflect best the toxic activity of nanoparticles [21]. Furthermore, nanosilver particles tend to agglomerate (flocculate) when dispersed in suspensions [22].

These limitations prevent a quantitative assessment of the antibacterial activity of nanosilver [14] to determine correct dose relations [23]. To overcome that, nanosilver particles with limited agglomeration and closely controlled size are needed [24]. One way to address this is to immobilize nanosilver on a support material [2,18]. That way, nanosilver is stabilized and retains its nanostructure since it is anchored on an inert support. Furthermore, having such immobilized nanosilver inhibits its flocculation in aqueous suspensions.

Several wet-chemistry based techniques have been used for synthesis of composite Ag/SiO_2 nanoparticles [25] or films [26] all of them exhibiting a strong antibacterial activity attributed to the release of Ag^+ ion through the porous SiO_2 matrix, typically made by such techniques. Alternatively, gas-phase (aerosol) routes for synthesis of sophisticated nanoparticles including Ag/SiO_2 offer several advantages over wet-chemistry routes: no creation of liquid by-products, easier collection of particles, fewer process steps, and the formation of high-purity products [27]. For large scale gas-phase manufacture of nanoparticles that involve the combustion of liquid precursors, for example flame-spray-pyrolysis (FSP), inexpensive inorganic precursors are preferred over organometallic ones [28]. However, inorganic precursors often do not form homogeneous particles [29,30]. This inhomogeneity has been observed also for flame-made metal clusters on ceramic particles (e.g. Pt-clusters supported on titania [31] or nanosilver on silica [2]) resulting in often bimodal metal size distributions. Therefore, there is a need to investigate the effect of the precursor composition on the morphology and antibacterial activity of nanosilver made from inexpensive inorganic precursors (e.g. Ag-nitrate) that are attractive for commercial synthesis of nanosilver [2,4].

Here, the focus is on exploring the effect of precursor composition on the characteristics of flame-made nanosilver-on-silica (Ag/SiO_2) particles made from inexpensive precursors that are typically used in industrial manufacture of nanosilver products [2]. So particle properties are systematically measured by S/TEM, EDX spectroscopy, XRD, N_2 adsorption and UV/vis spectroscopy while their antibacterial activity against the Gram-negative *Escherichia coli* (*E. coli*) is investigated in aqueous suspensions monitoring the released Ag^+ ion concentration. The antibacterial activity of such Ag/SiO_2 with bimodal Ag size distribution is compared to that with unimodal distribution [18]. Finally, a systematic comparison

between Ag mass, number and surface area concentrations for the antibacterial activity of nanosilver is made, investigating optimal dose-relations for risk assessments of nanosilver.

2. Experimental

2.1 Particle synthesis and characterization

Composite Ag/SiO_2 particles were made by FSP as described elsewhere [18]. Here, silver nitrate (Aldrich, purity > 99%) or silver acetate (Aldrich, purity >99%) and hexamethyldisiloxane (HMDSO, Aldrich, purity > 97%) or tetraethyl orthosilicate (TEOS, Aldrich, purity > 99%) were used as silver and silicon precursors, respectively [2,4,18]. For all precursor solutions the total metal (Ag + Si) concentration was 1 M. Silver nitrate and HMDSO were dissolved in 1:1 mixtures of ethanol (EtOH, Alcosuisse) and diethylene glycolmonobutyl ether (DEGBE, Aldrich, purity >98%), silver nitrate and TEOS were dissolved in 2-propanol (Aldrich, purity >98%) while silver acetate and HMDSO were dissolved in 2-ethylhexanoic acid (2-EHA, Aldrich, purity >98%) and acetonitrile (Aldrich, purity >98) in 1:1 ratio. All solutions were fed at 5 mL/min through the FSP nozzle [18] and dispersed by 5 L/min oxygen (Pan Gas, purity >99%). The Ag-content of the Ag/SiO_2 product particles was $x = 0 – 50$ wt% and noted as xAg/SiO_2. Their composition corresponds to the nominal Ag- and Si-content of the FSP precursor solution [4].

High resolution transmission electron microscopy (HRTEM) was performed on a CM30ST microscope (FEI; LaB6 cathode, at 300 kV, point resolution ~2 Å) and scanning transmission electron microscopy (STEM) on a Tecnai F30 (FEI; 300 kV) with a high-angle annular dark field (HAADF) detector with bright Z contrast and energy dispersive X-ray spectroscopy (EDXS; detector EDAX). Product particles were dispersed in ethanol and deposited onto a perforated carbon foil supported on a copper grid. Silver particle size distributions were obtained by counting at least 165 particles from S/TEM images. Nanosilver particle number and surface area concentrations in solution were calculated by multiplying the nanosilver number concentration and surface area (both estimated by the size distributions) with the nanosilver mass concentrations, respectively. X-ray diffraction (XRD) patterns were recorded with a Bruker D8 advance diffractometer (40 kV, 40 mA, CuK_α) at $2\theta = 20 - 70°$ with a step size 0.03°. Crystallite sizes were obtained by refined Rietveld Analysis on the (111) peak of Ag. The goodness-of-fit (GOF) was always below 1.2. Nitrogen adsorption-desorption isotherms were determined at 77 K and the specific surface area was derived using the Brunauer-Emmett-Teller (BET) method. The UV/vis optical absorption spectra were obtained with a Cary Varian 500. Particles were dispersed in de-ionized water at a concentration of 0.05 mg/mL by ultrasonication (Sonics vibra cell). The Ag^+ ion concentration of aqueous suspensions containing the xAg/SiO_2 nanoparticles was measured with an ion selective electrode and an ion meter (both Metrohm) [18].

2.2 Antibacterial activity

The antibacterial activity of the xAg/SiO_2 nanoparticles was obtained by a growth inhibition assay. *Escherichia coli* JM101 bacteria synthesizing a green fluorescent protein (GFP) from a plasmid-encoded gene were grown in Luria-Bertani (LB) broth at 37 °C overnight [32]. The culture was subsequently diluted with LB to an optical density (OD) of 0.05 at 600 nm, which corresponds to approximately 10^7 colony forming units (CFU)/mL. The xAg/SiO_2 nanoparticles were dispersed in de-ionized water by ultrasonication (Sonics vibra-cell) for 20 seconds at 75% amplitude with a pulse configuration on/off of 0.5s/0.5s. The nanoparticle suspensions were rather stable as determined by dynamic light scattering (Malvern Zetasizer, Nanoseries) and by monitoring their color that remained constant for more than a week and did not darken upon flocculation [18] as it commonly happens with nanosilver suspensions. For the assay, 50 μL of the aqueous suspensions containing the

Europe PMC Funders Author Manuscripts

dispersed Ag/SiO_2 nanoparticles were added to 50 μL of the diluted cells. The bacterial growth was monitored by the fluorescent signal of the GFP (Perkin Elmer 1420), corrected for background fluorescence and normalized to the control measurement (no particles). The error bars for each data point were the standard deviation of four measurements.

3. Results and Discussion

3.1 Effect of precursor composition

Figure 1 shows a STEM image and EDX spectra of two selected areas of a sample containing 1 wt% Ag (*1Ag/SiO2*) resulting from the Ag-acetate/HMDSO precursor. In the spectrum of area 1, comprising a relatively large bright spot as well as the gray area surrounding it, there are signals of Si and O corresponding to SiO_2 as well as of Ag confirming its presence there. In the spectrum of area 2 where the electron beam is focused on a gray area, only peaks of Si and O are present corresponding to amorphous SiO_2 [1]. So there are a few nanosilver particles (bright contrast) dispersed on an amorphous SiO_2 matrix (gray), characteristic morphology for flame-made noble-metals supported on ceramics nanoparticles [33,34]. Similar results were obtained for the product particles from different precursors and are consistent with prior flame-made Ag/SiO_2 nanoparticles [2,4,18]. The nanosilver particles are rather homogeneously dispersed on SiO_2 as it can be observed in Figure 2a where an STEM image of *10Ag/SiO2* coming from FSP of Ag-acetate/HMDSO is presented. In its inset, the nanosilver number size distribution (total 851 particles) is shown along with the number average nanosilver particle diameter (d_p) and the geometric standard deviation (σ_g). This distribution is substantially broader than other FSP-made noble metal clusters on ceramic supports [33]. This indicates that Ag clusters may have grown by coagulation as this $\sigma_g = 1.51$ is close to the self-preserving distribution of FSP-made particles [35] rather than grown-on-support particles [33]. It is quite possible that Ag metal and/or and SiO_2 form concurrently especially at the high Ag concentrations employed here.

Figure 2b shows a STEM image of the *10Ag/SiO2* nanoparticles from the Ag-nitrate/HMDSO precursor. Apart from the finely dispersed nanosilver particles (3-30 nm), there are also a few larger ones forming a second mode in nanosilver size distribution (inset) at 30-150 nm [2]. Similar bimodal Ag size distributions are obtained from FSP of Ag-nitrate/TEOS precursor solutions (Figure 2c) as with flame-made bimodal Pt clusters on TiO_2 [31]. The fine mode is attributed to nanosilver made by gas-to-particle conversion while the larger one is made by droplet-to-particle conversion, precipitation in precursor droplets prior to their full evaporation and combustion [36].

Figure 3a shows the XRD patterns of *25Ag/SiO2* made from the three different precursor solutions (Ag-acetate/HMDSO, Ag-nitrate/HMDSO, Ag-nitrate/TEOS). The peak positions of silver metal are also indicated. Even though all samples contain the same mass fraction of nanosilver, the main diffraction peak is broader for that coming from the Ag-acetate solution indicating smaller nanosilver. For both samples that exhibit a bimodal nanosilver particle size distribution (Fig. 2b,c) the peaks are quite sharper since larger particles are also detected. It should be noted that XRD is not suitable for detection of silver oxide layers on the nanosilver surface. It is quite likely that such layers are there [1,13,18] as has been shown very recently by EXAFS [37].

Table 1 shows that nanosilver crystals made from Ag-acetate/HMDSO are unimodal, so one crystal size is estimated from the XRD spectra (Figure 3a). For Ag-contents $x < 10$ wt% the crystal concentration was below the XRD detection limit. For an increasing Ag-content x, larger nanosilver crystal sizes are formed [18]. For nanosilver made from Ag-nitrate/HMDSO, however, two average crystal sizes can be estimated, with the mass fraction of the larger mode being approximately 20 %. Remarkably, when the samples resulting from FSP

of the Ag-nitrate/TEOS are fitted with two crystal sizes, only the larger mode can be estimated reliably as the fine crystals were too small for detection by XRD. Since nanosilver made from Ag-nitrate/TEOS could not be quantitatively distinguished, no further experiments with this precursor composition were carried out.

The observed bimodality of nanosilver made from Ag-nitrate can also be verified by the optical absorption spectra of the dispersed *xAg/SiO2* nanoparticles from all three precursor solutions. Figure 3b shows exemplarily these spectra of aqueous suspensions containing the *25Ag/SiO2* nanoparticles. The characteristic silver plasmon absorption band around 400 nm is normalized for all samples and can be clearly distinguished [5,22]. The presence of larger nanosilver particles when made from Ag-nitrate (dotted and broken lines) can be verified by the peak position of their plasmon absorption bands [5]. These have been shifted to higher wavelengths than those made from Ag-acetate (solid line). In addition, the presence of larger particles in the tail of the nanosilver particle size distribution made from Ag-nitrate (resulting from the bimodality) can also be detected since these spectra are wider than the one of the nanosilver made from Ag-acetate [5].

Figure 4a shows a representative TEM image of the *10Ag/SiO2* from the Ag-acetate/HMDSO precursor with the interdispersed nanosilver particles (dark) on the amorphous silica (gray) support [18]. Figure 4b shows the N_2 adsorption-desorption isotherm of the *2Ag/SiO2* nanoparticles as representative example showing the typical hysteresis curve for non-porous particles [38]. As inset, the corresponding TEM image is shown. Figures 4c-h show the nanosilver particle size distributions counting 165-851 Ag particles [18] as determined by the S/TEM analysis having the characteristic lognormal shape of aerosol-made nanomaterials. Such size distributions are employed to estimate an average nanosilver size, especially for the lower Ag-contents *x*, which could not be detected by XRD (Table 1). The average nanosilver particle diameter increases with increasing Ag-content *x* in the *xAg/SiO2* particles from 4 to 9 nm [18]. This control over nanosilver size, in addition to the fact that it is immobilized on nanostructured SiO_2, makes possible the investigation of the antibacterial activity of nanosilver without artifacts arising from its flocculation or agglomeration.

Figure 5 shows the specific surface area (SSA) of *xAg/SiO2* particles as a function of Ag-content *x*. For pure SiO_2 (x = 0 wt%) the samples have 250-300 m^2/g which corresponds to an average silica primary particle diameter of ~9 to 11 nm, in agreement with literature [39]. For increasing *x* (1-10 wt%), however, there is an increase in the total SSA. This indicates that the presence of Ag in the product particles affects the growth of SiO_2, perhaps by formation of a solid solution at very low Ag-contents, as it has been observed also with trace contents of SiO_2-based mixed oxides [39]. Another possibility is the presence of Ag atoms to act as seeds for SiO_2 nucleation and thus to affect the nucleation kinetics of SiO_2 clusters. Increasing *x* further, decreases the SSA monotonically, as the presence of Ag (being a higher density material than SiO_2) is significant. It should be noted that even for the highest Ag-contents here, the total SSA originates mostly from SiO_2 as that attributed to nanosilver as determined by TEM [18] is only 0.26 - 4.5 % for *x* = 1 - 25 wt%. So, all samples have high SSA regardless of precursor composition, a desired property [40] when such particles are employed as fillers in textiles [2] or polymers [4].

3.2 Antibacterial activity

The antibacterial activity of nanosilver is investigated by monitoring the fluorescence intensity of suspensions of *E. coli* cells (that directly correlates with their population [18]) at 37 °C for 330 minutes which encode the green fluorescent protein (GFP). Figure 6a shows the *E. coli* growth in the presence of *10Ag/SiO2* made from Ag-acetate/HMDSO at various Ag mass concentration (*C* = 0-1.6 mg/L of Ag). The experimental uncertainty of these *E.*

coli growth data is within the error bar, which was similar for all data points. The characteristic exponential *E. coli* growth evolution in the absence of particles (stars) and presence of pure SiO_2 (hexagons) is identical proving that SiO_2 alone does not influence bacterial growth [18]. When *10Ag/SiO2* composite nanoparticles are present in suspension, the fluorescence was reduced for increased nanosilver concentration (C = 0.4-1.6 mg/L) indicating its antibacterial activity. Figure 6b shows *E. coli* growth curves in the presence of *xAg/SiO2* nanoparticles made from Ag-acetate/HMDSO at C = 0.1-2.5 mg/L of Ag (all samples have 10 mg/L of the composite *xAg/SiO2* nanoparticles). For both Figures 6a,b the bacterial growth is inhibited for the highest Ag content and Ag mass concentration. The released Ag^+ ions dominate the antibacterial activity of nanosilver for the employed sizes here [18] in agreement with literature [13,41,42] and showing a stronger antibacterial activity for higher Ag mass concentration.

Figure 7a shows the final (after 330 minutes) *E. coli* growth % as a function of x for *xAg/SiO2* particles made from bimodal Ag-nitrate/HMDSO (triangles) and unimodal Ag-acetate/HMDSO (circles). The Ag mass concentration applied was C = 1 (open symbols) and 2 mg/L (filled symbols), respectively. The 100 *% E. coli* growth has been estimated as the value of the control (Fig. 6, stars). The lower Ag-content x samples exhibit stronger antibacterial activity with very similar *E. coli* growth regardless of precursor composition. This indicates that, first, smaller nanosilver particles are more active than larger ones because of their higher surface area [14,18] and second, the larger mode of bimodal nanosilver (made from Ag-nitrate) does not really contribute much in its antibacterial activity.

Figure 7b shows the Ag^+ ion concentration [Ag^+] of aqueous suspensions containing *xAg/SiO2* nanoparticles (20 mg/L of Ag) made from Ag-nitrate/HMDSO (triangles) and Ag-acetate/HMDSO (circles, from [18]) as a function of the Ag-content x. The top axis shows the concentration of xAg/SiO_2 nanoparticles in solution. For both samples the [Ag^+] is similar and higher for the lower Ag-content x samples. This is attributed to the smaller nanosilver size of these samples [18]. Nanosilver smaller than 10 nm (size range of the smaller mode, Figure 2b) releases Ag^+ ions from its surface that have much higher antibacterial activity than from direct bacterial contact with that surface [18]. Thus, when two modes are present, the particles of the smaller one will release more Ag^+ ions. As seen from XRD (Table 1) of nanosilver made from Ag-nitrate/HMDSO solutions, the large Ag-crystal mode consists of about 20 wt% of the total Ag. This fraction contributes ~5 % to surface area. Therefore, even though this nanosilver is bimodal its surface area is dominated by the smaller particles so its antibacterial activity is similar to that of unimodal nanosilver. This indicates that the nanosilver surface area plays quite an important role for its antibacterial activity. It should be noted, however, that if the mass fraction of the larger mode would be significantly larger, then the Ag antibacterial activity would be influenced also by the larger particles [18].

Figure 6 also shows the exposed nanosilver surface area concentration ($C{\cdot}AgSSA$) as calculated by the Ag mass concentration C and Ag SSA (obtained from the Ag size distributions in Fig. 4c-h). Now, if one selects the *E. coli* growth curves of Fig. 6a,b with similar nanosilver surface area concentration, $C{\cdot}AgSSA$: 21.6/15.2 (triangles), 43.2/40.2 (diamonds) and 86.4/90.0·10^{-3} m^2/L (squares), they overlap within their measurement error. In fact, when the *E. coli* growth data in the presence of nanosilver made from Ag-acetate/HMDSO of Fig. 6 and Fig. 7a (Fig. 8, open: 210, half-filled: 270, filled symbols: after 330 minutes) are normalized to the control growth curve (stars) and plotted as a function of $C{\cdot}AgSSA$ (Fig. 8a), they fall on a straight line (R^2 = 0.90) excluding data with minimal *E. coli* growth (< 10%) as their growth period becomes too uncertain. This indicates that indeed the antibacterial activity of nanosilver depends on its exposed surface area concentration and it is time independent as this holds for all three time periods. This dependency originates

from the released Ag^+ ions from the nanosilver surface [18]. Such a relation can be difficult to observe when nanosilver that has its surface modified [19] is employed which may influence the Ag^+ ion release as well as the bacterial contact with its surface [18].

Now Figure 8b shows exactly the same *E. coli* data as a function of Ag mass concentration, *C*. Clearly these data are much more scattered ($R^2 = 0.56$, again excluding from the regression data with *E. coli* growth < 10%). Most notably, for the same Ag mass concentration of $C = 1$ mg/L (circles), the *E. coli* growth covers the entire spectrum; from complete inhibition to nearly full *E. coli* growth. This highlights best the limitations of using mass or molar concentrations to assess the nanosilver dose relations for its antibacterial activity. When the nanosilver particle number concentration is calculated (Figure 8c) the data are less scattered than for the Ag mass concentration (Figure 8b) indicating that number concentration also is advantageous over mass concentration for nanosilver. However, when the data are plotted as a function of the surface area concentration (Figure 8a), they are the least scattered, verifying that indeed the correct dose relations for the antibacterial activity of nanosilver particles is best reflected when surface area concentrations are used.

4. Conclusions

Nanosilver particles were made and immobilized on nanostructured SiO_2 by spray combustion (flame spray pyrolysis, FSP) of three different precursor solutions. The effect of precursor composition on the characteristics of product Ag/SiO_2 nanoparticles was investigated. Nanosilver made by FSP of Ag-acetate and HMDSO showed a unimodal size distribution, while that made from Ag-nitrate and HMDSO or TEOS precursor solutions exhibited a bimodal size distributions. The antibacterial activity of these composite Ag/SiO_2 nanoparticles was investigated against *E. coli* bacteria. Nanosilver made from inexpensive Ag-nitrate had similar antibacterial activity to that made from Ag-acetate as the fine mode of the distribution dominated its bactericidal properties by releasing or leaching of silver ions. Additionally, the nanosilver surface area concentration in suspension correlates best with Ag antibacterial activity rather than with nanosilver mass/molar or number concentration. This indicates that the nanosilver dose expressions in toxicological studies might be most accurate when assessed in terms of surface area concentrations of nanosilver.

Acknowledgments

Support by the Swiss National Science Foundation (#200020-126694) and the European Research Council is gratefully acknowledged.

References

[1]. Hannemann S, Grunwaldt JD, Krumeich F, Kappen P, Baiker A. Electron microscopy and EXAFS studies on oxide-supported gold-silver nanoparticles prepared by flame spray pyrolysis. Appl. Surf. Sci. 2006; 252:7862–7873.

[2]. Height, MJ.; Pratsinis, SE. Antimicrobial and antifungal powders made by flame spray pyrolysis. Eur. Patent, EP1846327 (A1). 2007.

[3]. Morones JR, Elechiguerra JL, Camacho A, Holt K, Kouri JB, Ramirez JT, Yacaman MJ. The bactericidal effect of silver nanoparticles. Nanotechnology. 2005; 16:2346–2353. [PubMed: 20818017]

[4]. Loher S, Schneider OD, Maienfisch T, Bokorny S, Stark WJ. Micro-organism-triggered release of silver nanoparticles from biodegradable oxide carriers allows preparation of self-sterilizing polymer surfaces. Small. 2008; 4:824–832. [PubMed: 18416429]

[5]. Willets KA, Van Duyne RP. Localized surface plasmon resonance spectroscopy and sensing. Annu. Rev. Phys. Chem. 2007; 58:267–297. [PubMed: 17067281]

[6]. Quinten M. The color of finely dispersed nanoparticles. Appl. Phys. B-Lasers Opt. 2001; 73:317–326.

[7]. Lee PC, Meisel D. Adsorption and surface-enhanced Raman of dyes on silver and gold sols. J. Phys. Chem. 1982; 86:3391–3395.

[8]. Lee BG, Griscom SB, Lee JS, Choi HJ, Koh CH, Luoma SN, Fisher NS. Influences of dietary uptake and reactive sulfides on metal bioavailability from aquatic sediments. Science. 2000; 287:282–284. [PubMed: 10634777]

[9]. Erickson BE. Nanosilver pesticides. Chem. Eng. News. 2009; 87(48):25–26.

[10]. Auffan M, Rose J, Bottero J-Y, Lowry GV, Jolivet J-P, Wiesner MR. Towards a definition of inorganic nanoparticles from an environmental, health and safety perspective. Nature Nanotechnol. 2009; 4:634–641. [PubMed: 19809453]

[11]. Wijnhoven SWP, Peijnenburg WJGM, Herberts CA, Hagens WI, Oomen AG, Heugens EHW, Roszek B, Bisschops J, Gosens I, Van De Meent D, Dekkers S, De Jong WH, van Zijverden M, Sips A.n.J.A.M. Geertsma RE. Nano-silver - a review of available data and knowledge gaps in human and environmental risk assessment. Nanotoxicology. 2009; 3:109–138.

[12]. Tolaymat TM, El Badawy AM, Genaidy A, Scheckel KG, Luxton TP, Suidan M. An evidence-based environmental perspective of manufactured silver nanoparticle in syntheses and applications: A systematic review and critical appraisal of peer-reviewed scientific papers. Sci. Total Environ. 2010; 408:999–1006. [PubMed: 19945151]

[13]. Gunawan C, Teoh WY, Marquis CP, Lifia J, Amal R. Reversible antimicrobial photoswitching in nanosilver. Small. 2009; 5:341–344. [PubMed: 19152359]

[14]. Lok CN, Ho CM, Chen R, He QY, Yu WY, Sun H, Tam PKH, Chiu JF, Che CM. Silver nanoparticles: partial oxidation and antibacterial activities. J. Biol. Inorg. Chem. 2007; 12:527–534. [PubMed: 17353996]

[15]. Lide, DR., editor. CRC Handbook of Chemistry and Physics. 89 (Internet version) ed.. CRC Press/Taylor and Francis; Boca Raton, FL: 2010.

[16]. Benn TM, Westerhoff P. Nanoparticle silver released into water from commercially available sock fabrics. Environ. Sci. Technol. 2008; 42:4133–4139. [PubMed: 18589977]

[17]. Navarro E, Piccapietra F, Wagner B, Marconi F, Kaegi R, Odzak N, Sigg L, Behra R. Toxicity of silver nanoparticles to Chlamydomonas reinhardtii. Environ. Sci. Technol. 2008; 42:8959–8964. [PubMed: 19192825]

[18]. Sotiriou GA, Pratsinis SE. Antibacterial activity of nanosilver ions and particles. Environ. Sci. Technol. 2010; 44:5649–5654. [PubMed: 20583805]

[19]. Carlson C, Hussain SM, Schrand AM, Braydich-Stolle LK, Hess KL, Jones RL, Schlager JJ. Unique cellular interaction of silver nanoparticles: size-dependent generation of reactive oxygen species. J. Phys. Chem. B. 2008; 112:13608–13619. [PubMed: 18831567]

[20]. Oberdorster G, Stone V, Donaldson K. Toxicology of nanoparticles: A historical perspective. Nanotoxicology. 2007; 1:2–25.

[21]. Nel A, Xia T, Madler L, Li N. Toxic potential of materials at the nanolevel. Science. 2006; 311:622–627. [PubMed: 16456071]

[22]. Sotiriou GA, Sannomiya T, Teleki A, Krumeich F, Vörös J, Pratsinis SE. Non-Toxic Dry-Coated Nanosilver for Plasmonic Biosensors. Adv. Funct. Mater. 2010; 20:4250–4257.

[23]. Owen R, Handy R. Formulating the problems for environmental risk assessment of nanomaterials. Environ. Sci. Technol. 2007; 41:5582–5588. [PubMed: 17874758]

[24]. Stone V, Nowack B, Baun A, van den Brink N, von der Kammer F, Dusinska M, Handy R, Hankin S, Hassellov M, Joner E, Fernandes TF. Nanomaterials for environmental studies: Classification, reference material issues, and strategies for physico-chemical characterisation. Sci. Total Environ. 2010; 408:1745–1754. [PubMed: 19903569]

[25]. Kim YH, Lee DK, Cha HG, Kim CW, Kang YS. Synthesis and characterization of antibacterial Ag-SiO_2 nanocomposite. J. Phys. Chem. C. 2007; 111:3629–3635.

[26]. Jeon HJ, Yi SC, Oh SG. Preparation and antibacterial effects of Ag-SiO_2 thin films by sol-gel method. Biomaterials. 2003; 24:4921–4928. [PubMed: 14559005]

[27]. Pratsinis SE, Mastrangelo SVR. Material synthesis in aerosol reactors. Chem. Eng. Prog. 1989; 85:62–66.

[28]. Jossen R, Mueller R, Pratsinis SE, Watson M, Akhtar MK. Morphology and composition of spray-flame-made yttria-stabilized zirconia nanoparticles. Nanotechnology. 2005; 16:S609–S617. [PubMed: 21727483]

[29]. Jossen R, Pratsinis SE, Stark WJ, Madler L. Criteria for flame-spray synthesis of hollow, shell-like, or inhomogeneous oxides. J. Am. Ceram. Soc. 2005; 88:1388–1393.

[30]. Madler L, Pratsinis SE. Bismuth oxide nanoparticles by flame spray pyrolysis. J. Am. Ceram. Soc. 2002; 85:1713–1718.

[31]. Schulz H, Madler L, Strobel R, Jossen R, Pratsinis SE, Johannessen T. Independent control of metal cluster and ceramic particle characteristics during one-step synthesis of Pt/TiO_2. J. Mater. Res. 2005; 20:2568–2577.

[32]. Sambrook, J.; Russell, DW. Molecular Cloning: A Laboratory Manual. 3ed.. NY Cold Spring Harbor Laboratory Press: Cold Spring Harbor; 2001.

[33]. Madler L, Stark WJ, Pratsinis SE. Simultaneous deposition of Au nanoparticles during flame synthesis of TiO_2 and SiO_2. J. Mater. Res. 2003; 18:115–120.

[34]. Strobel R, Stark WJ, Madler L, Pratsinis SE, Baiker A. Flame-made platinum/alumina: structural properties and catalytic behaviour in enantioselective hydrogenation. J. Catal. 2003; 213:296–304.

[35]. Mueller R, Jossen R, Kammler HK, Pratsinis SE, Akhtar MK. Growth of zirconia particles made by flame spray pyrolysis. AIChE J. 2004; 50:3085–3094.

[36]. Madler L, Stark WJ, Pratsinis SE. Flame-made ceria nanoparticles. J. Mater. Res. 2002; 17:1356–1362.

[37]. Beier MJ, Schimmoeller B, Hansen TW, Andersen JET, Pratsinis SE, Grunwaldt JD. Selective side-chain oxidation of alkyl aromatic compounds catalyzed by cerium modified silver catalysts. J. Molec. Catal. A-Chem. 2010; 331:40–49.

[38]. Schimmoeller B, Hoxha F, Mallat T, Krumeich F, Pratsinis SE, Baiker A. Fine tuning the surface acid/base properties of single step flame-made Pt/alumina. Appl. Catal. A-Gen. 2010; 374:48–57.

[39]. Schulz H, Madler L, Pratsinis SE, Burtscher P, Moszner N. Transparent nanocomposites of radiopaque, flame-made Ta_2O_5/SiO_2 particles in an acrylic matrix. Adv. Funct. Mater. 2005; 15:830–837.

[40]. Camenzind A, Caseri WR, Pratsinis SE. Flame-made nanoparticles for nanocomposites. Nano Today. 2010; 5:48–65.

[41]. Li P, Li J, Wu CZ, Wu QS. Synergistic antibacterial effects of beta-lactam antibiotic combined with silver nanoparticles. Nanotechnology. 2005; 16:1912–1917.

[42]. Tiwari DK, Behari J, Sen P. Time and dose-dependent antimicrobial potential of Ag nanoparticles synthesized by top-down approach. Curr. Sci. 2008; 95:647–655.

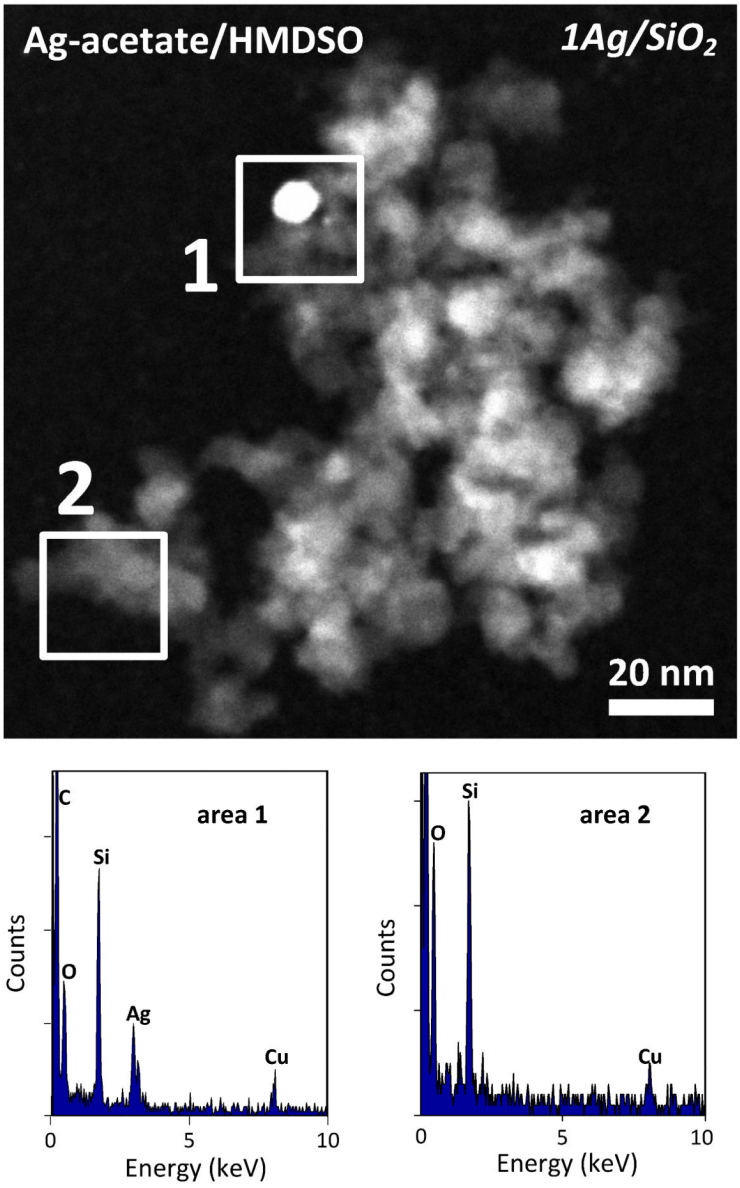

Fig. 1.
STEM image of *1Ag/SiO2* nanoparticles and EDX spectra of the selected areas (the C and Cu peaks arise from the carbon coated copper grid).

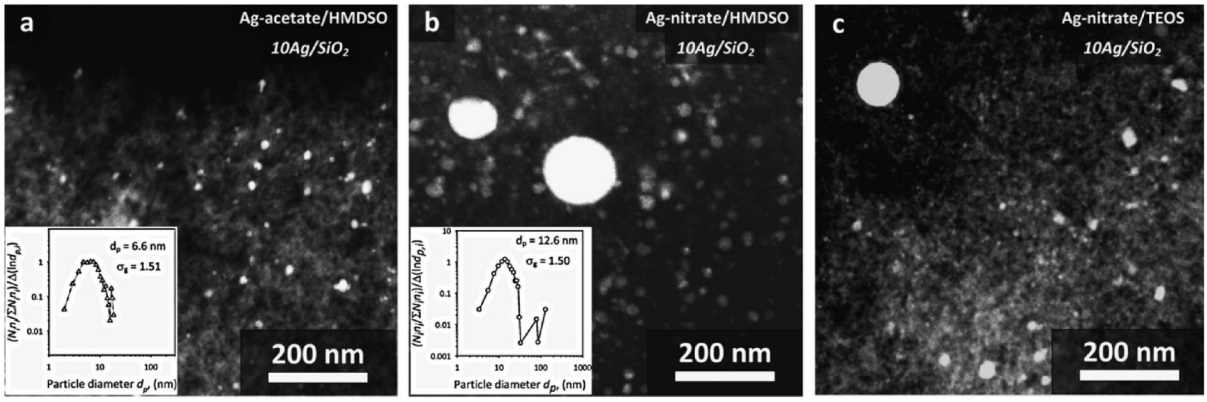

Fig. 2.

STEM images of *10Ag/SiO*$_2$ resulting from the three different precursor compositions (a: Ag-acetate/HMDSO, b: Ag-nitrate/HMDSO, c: Ag-nitrate/TEOS) presenting the dispersed nanosilver particles on the amorphous nanostructured silica. Nanosilver particles resulting from Ag-nitrate precursors have a bimodal size distribution, while for the ones from Ag-acetate have a unimodal one. In the insets, the nanosilver particle number size distributions are shown with their average particle diameter d_p and geometric standard deviation σ_g.

Europe PMC Funders Author Manuscripts

Europe PMC Funders Author Manuscripts

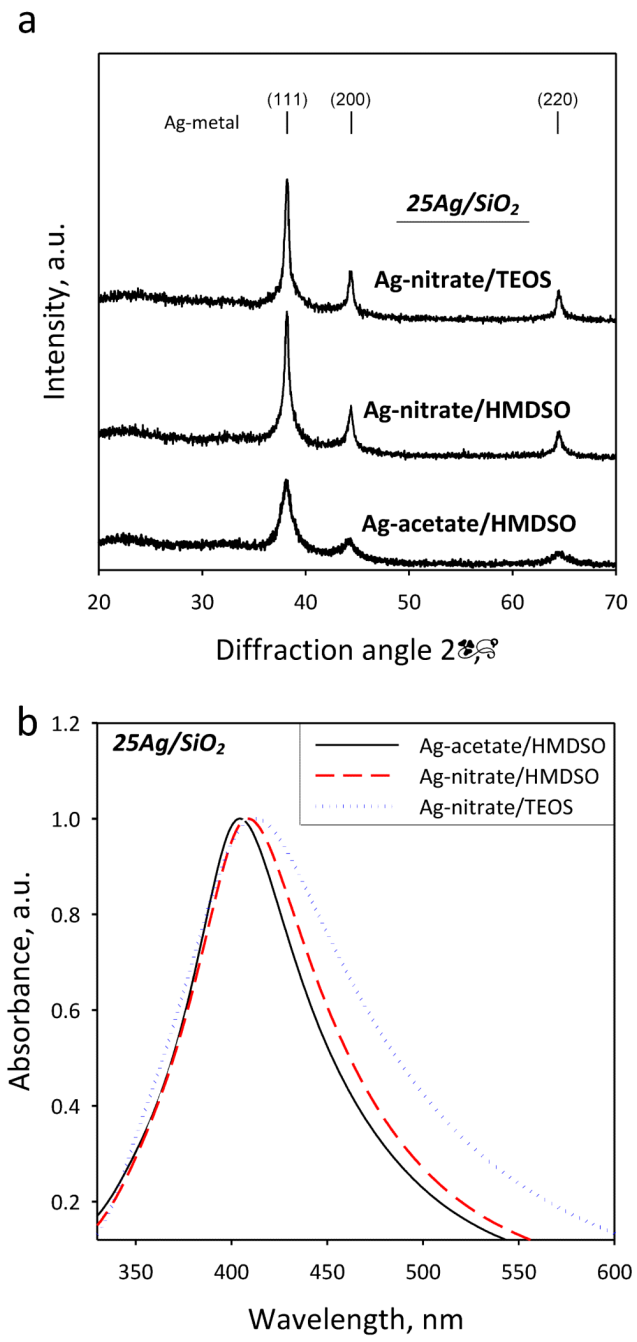

Fig. 3.

(a) XRD patterns of the *25Ag/SiO2* composite nanoparticles resulting from FSP of three different precursor compositions. Sharp Ag peaks with broad base indicate a bimodal crystal size distribution [29] and come here from FSP of Ag-nitrate solutions. (b) Optical absorption spectra of aqueous suspensions containing the *25Ag/SiO2* nanoparticles made by FSP from all precursor solutions. The peak position of the plasmon absorption band is red-shifted for larger nanosilver particles and the bands are broader for nanosilver with bimodal size distributions made by FSP of inexpensive Ag-nitrate precursors (dotted and broken lines).

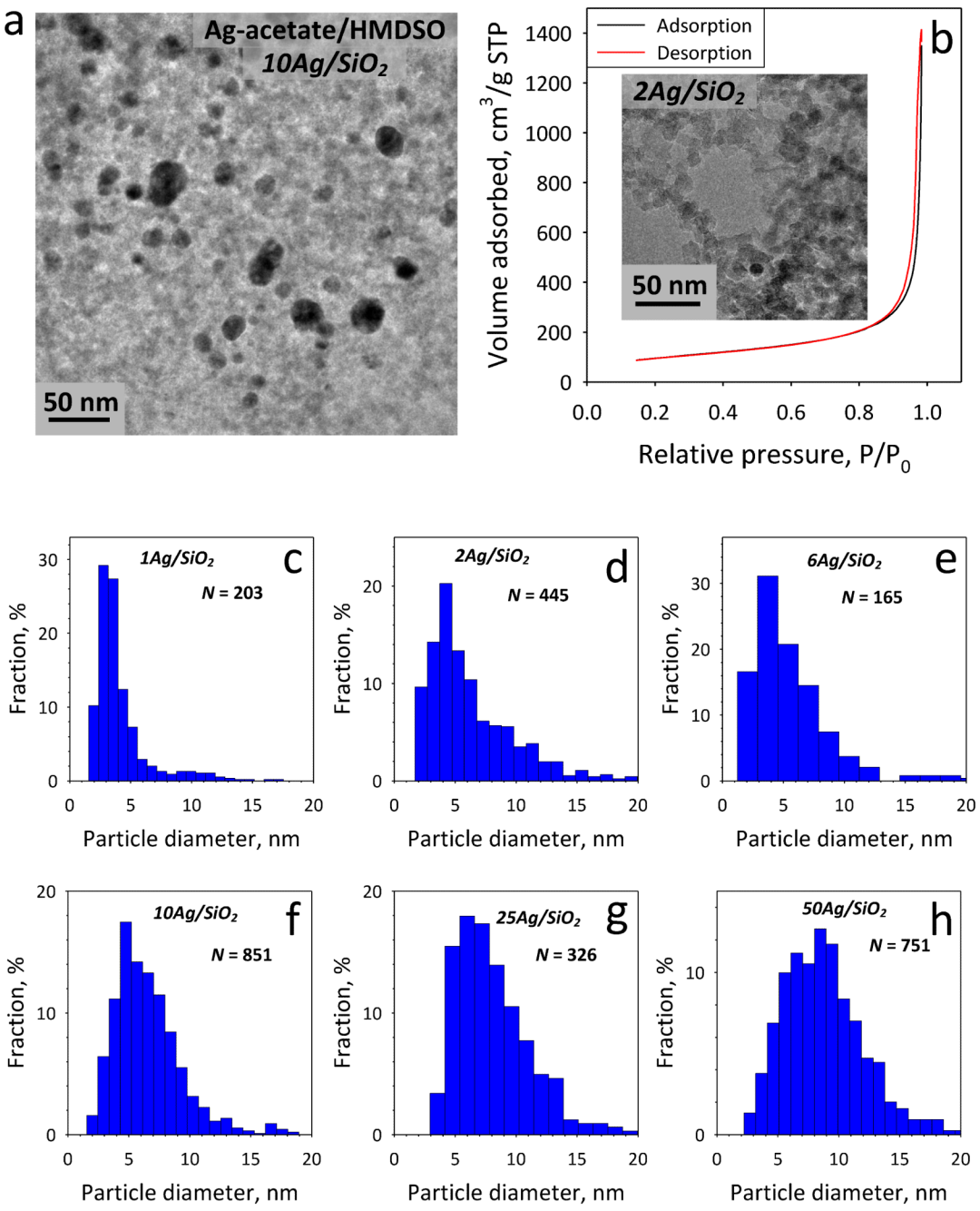

Fig. 4.

(a) TEM image of the *10Ag/SiO2* made from FSP of Ag-acetate solutions showing nanosilver (dark) particles dispersed on amorphous (gray) *SiO2* support. (b) The N_2 adsorption-desorption curve for the *2Ag/SiO2* nanoparticles. As inset the corresponding TEM image is shown. (c-h) Counted Ag particle size distributions for all samples from S/TEM.

Europe PMC Funders Author Manuscripts

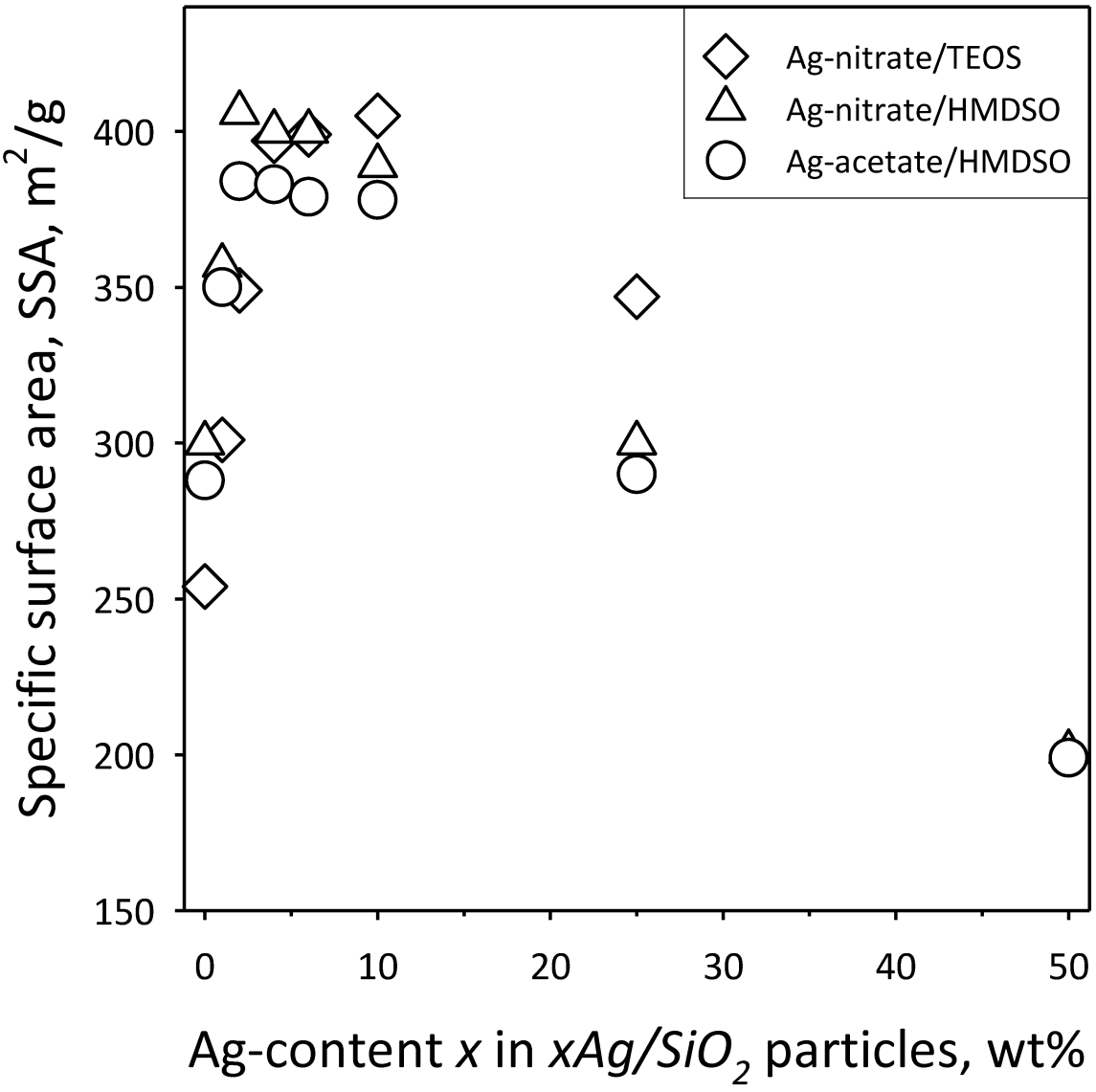

Fig. 5.

The specific surface area (SSA) of composite xAg/SiO_2 nanoparticles as a function of the Ag-content *x (wt%)*, for samples made from FSP of Ag-nitrate/TEOS (diamonds), Ag-nitrate/HMDSO (triangles) and Ag-acetate/HMDSO (circles).

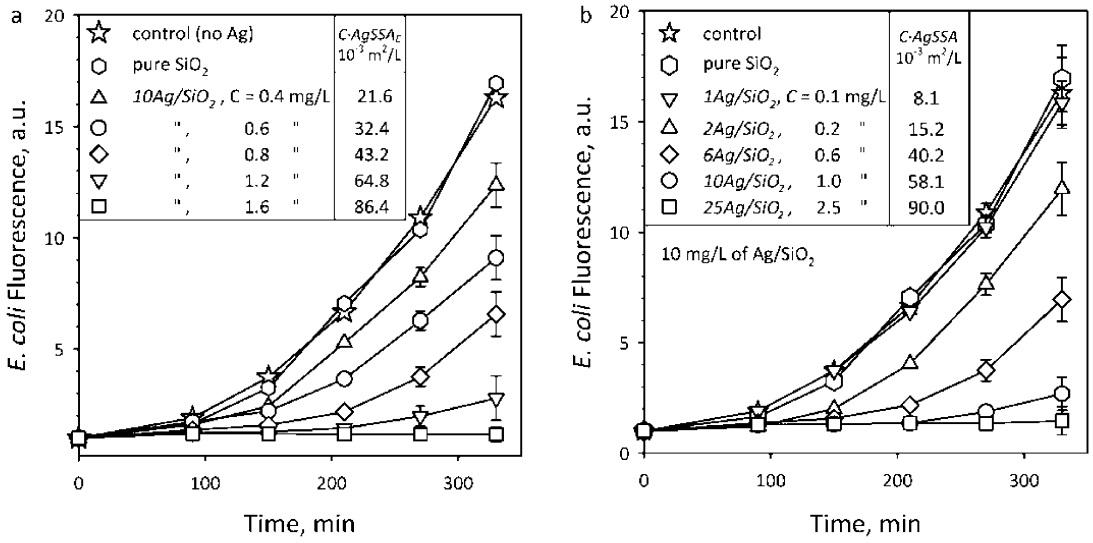

Fig. 6.

Nanosilver toxicity against *E. coli*. The evolution of *E. coli* growth (fluorescence) for 330 minutes at 37 °C in the presence of (a) *10Ag/SiO2* particles (C = 0-1.6 mg/L of Ag) and (b) *xAg/SiO2* for Ag-contents x = 0-25 wt% and Ag mass concentrations C = 0.1-2.5 mg/L. The experimental uncertainty of the data is within the error bar, which was similar for all final data points. The corresponding silver surface area concentration (*C·AgSSA*) in these suspensions is also presented.

Europe PMC Funders Author Manuscripts

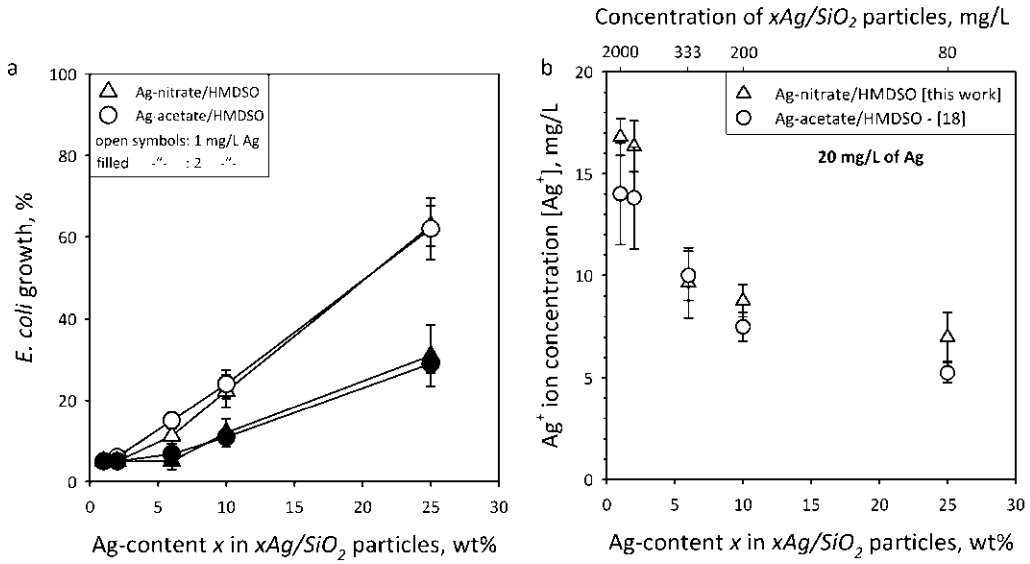

Fig. 7.

(a) The final (after 330 minutes) *E. coli* growth % as a function of the Ag-content *x* in the xAg/SiO_2 particles in the presence of 1 (open symbols) and 2 mg/L (filled symbols) Ag mass concentration from bimodal (triangles) and unimodal (circles) nanosilver made by FSP of Ag-nitrate (triangles) and –acetate (circles), respectively, precursor solutions. The *E. coli* growth has been normalized to the 100% curve from Fig. 6. The lower Ag-content *x* samples exhibit stronger antibacterial activity with very similar *E. coli* growth independently of the precursor. This indicates first that smaller nanosilver particles are more active than larger ones, and second that the large mode of the bimodal nanosilver does not influence its antibacterial activity as that mode contributes rather little on the nanosilver surface area here. (b) The Ag^+ ion concentration $[Ag^+]$ of aqueous suspensions containing the xAg/SiO_2 nanoparticles (20 mg/L of Ag) made from Ag-nitrate/HMDSO (triangles) and Ag-acetate/HMDSO (circles, from [18]) as a function of the Ag-content *x*. The top axis shows the concentration of xAg/SiO_2 nanoparticles in solution.

Europe PMC Funders Author Manuscripts

Europe PMC Funders Author Manuscripts

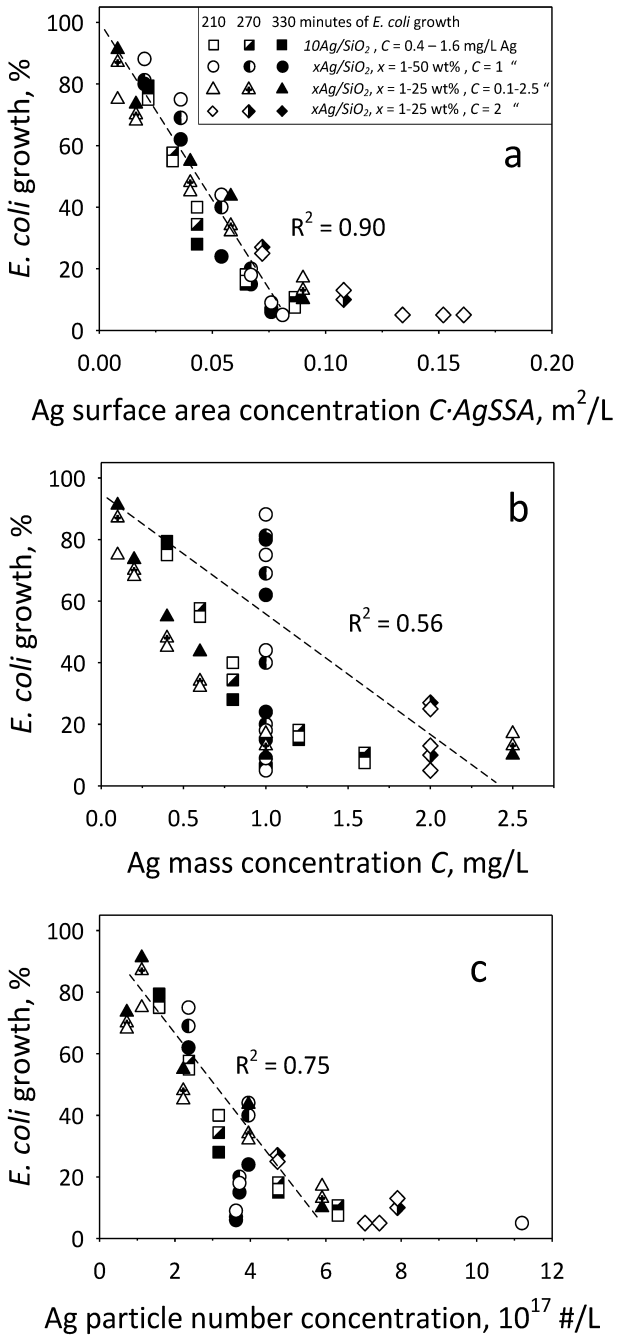

Fig. 8.

Antibacterial activity and surface area concentration of nanosilver. The extent of *E. coli* growth of all data at 210, 270 and 330 minutes as a function of the Ag (a) surface area concentration *C·AgSSA*, (b) mass concentration *C* in suspension and (c) nanosilver particle number concentration. The vast variability of *E. coli* growth at identical Ag mass (or molar) concentration in contrast to Ag surface area concentration points out the limitation of using Ag mass concentration in assessing the antibacterial activity of nanosilver in liquid suspensions.

Europe PMC Funders Author Manuscripts

Table 1

XRD analysis of nanosilver made by FSP of the three different precursor compositions with the distribution mode, average crystal size (d_{XRD}) and corresponding weight fraction (wt%) of the small (s) and large (l) mode of the Ag crystal size distribution.

Ag-nitrate/HMDSO in EtOH-DEGBE				**Ag-acetate/HMDSO in Acetonitrile-2-EHA**		**Ag-nitrate/TEOS in 2-propanol**	
Ag-content *x* in *xAg/SiO$_2$*	**mode**	**d_{XRD} (nm) s:small, l:large**	**wt%**	**mode**	**d_{XRD} (nm)**	**mode**	**d_{XRD} (nm)**
10	bimodal	s: 5.7 ± 1.6 l: 25.3 ± 2.0	70 ± 15 % 30 ± 15 %	unimodal	6.9 ± 0.9	bimodal by STEM	s: undefined l: 20.9 ± 2.1
25	bimodal	s: 7.1 ± 1.0 l: 53.6 ± 14.9	80 ± 2 % 20 ± 2 %	unimodal	8.1 ± 0.8	bimodal by STEM	s: undefined l: 23.7 ± 1.8
50	bimodal	s: 8.6 ± 1.2 l: 40.6 ± 10.6	82 ± 1 % 18 ± 1 %	unimodal	8.7 ± 0.6	not	prepared